First principles calculations and experimental study of the optical properties of Ni-doped ZnS

Materials Research Express

OPEN ACCESS

RECEIVED
3 October 2019

REVISED
9 November 2019

ACCEPTED FOR PUBLICATION
28 November 2019

PUBLISHED
9 December 2019

PAPER

First principles calculations and experimental study of the optical properties of Ni-doped ZnS

S Rodríguez[1], C Zandalazini[1], J Navarro[1], K T Vadiraj[2] and E A Albanesi[1,3]

[1] Instituto de Física del Litoral (IFIS Litoral-CONICET-UNL), Güemes 3450, 3000, Santa Fe, Argentina
[2] Department of Studies in Environmental Science, Manasagangotri, University of Mysore, Mysore 570 006, India
[3] Facultad de Ingeniería, Universidad Nacional de Entre Ríos, 3101, Oro Verde, Entre Ríos, Argentina

E-mail: sindy.rodriguez@santafe-conicet.gov.ar

Keywords: zinc sulphide doped with nickel, XRD, XPS, DFT, Hubbard potential

Abstract

Zinc sulphide doped with nickel (Ni:ZnS) has many applications in different fields like materials science, electronics, optics, and other industrial applications. Experimentally, a large variety of methods have been developed for Ni:ZnS synthesizing, where the chemical synthesis with capping agent is most successful, but has disadvantages like purity and the low performance. In addition, since there is not also much theoretical information about its features, the electronic and optical response of Ni:ZnS were studied, both experimentally by x-ray diffractometry (XRD), transmission electron microscopy (HR-TEM), and x-ray photoelectron spectroscopy (XPS) and theoretically by means of the density functional theory (DFT) calculations, giving an unified understanding of the electrooptical performance of this compound. In the same way, the importance of the inclusion of Ni impurities in the structure was studied and analyzed by the inclusion of a Hubbard potential in the calculations. We found that the optimal U value for Ni atoms is 4 eV in agreement with experimental results obtained by XPS. The dielectric function (ε_2) for pure and doped systems showed that the influence of the Ni atom is mainly given in the range of low energy regions ($E < 6$ eV), where the new peaks are associated to transitions that include the impurity band states.

1. Introduction

ZnS is a II–VI intrinsic semiconductor with excellent chemical and physical properties like wide band-gap energy of 3.7 eV at room temperature, high optical transmittances in the visible region, large Bohr exciton radius (2.5 nm) and large exciton binding energy (40 meV) [1, 2]. Due to its versatility the ZnS has become a promising material for many areas of research including light emitting diode (LED), solar cell, active sensor as well as wastewater treatment, electro-luminescent displays, antireflection coating for infrared devices and other nonlinear optical devices among others [3–5]. The structural properties of ZnS are easily to be tailored by means of reducing their dimensions or generating chemical modifications. The ZnS can be designed in several dimensions, ranging from 3D, 2D, 1D structures to 0D structure of quantum dots, where the drastic reduction in the material size change their band structure (the band gap increases as the particle size decreases, with this edge of band splits and create discrete energy levels) [6, 7]. On the other hand, the doping of ZnS, has been extensively performed in the last decades determining that the impurity plays a very important role in the efficiency and position of the emission bands [8]. Luminescent properties of ZnS can be controlled using various dopants such as Ni, Fe, Mn, Cu etc [9]. Bera *et al* [10] prepared pure ZnS and Mn-doped ZnS using hydrothermal synthesis. In their work, the photoluminescence (PL) spectra shows a strong peak from doped ZnS since it contains an effective Mn luminescence center [10]. Furthermore, Kumar and co-workers reported that the photoluminescence emission decreases with increase in Ni concentration for the Ni-doped ZnS quantum dots —prepared by chemical precipitation method—[1]. Other properties, such as electroluminescence (EL) and cathode luminescence (CL) are found to be of great interest. So far, pristine ZnS properties have been extensively studied experimentally [11] and theoretically [12, 13]. In contrast, the theoretical study of doped systems,

especially those doped with 3d elements, have been less investigated (works that include the Hubbard Coefficient corrections for the strongly correlated states). In this work we included both, the experimental and the theoretical study of the electronic and optical properties of Zinc sulphide doped with Nickel, including also the photoemission spectra of Ni:ZnS. In this way, we obtained the optical excitations at different wavelengths which are useful to identify the role of the dopant agents in the properties of the doped material, in comparison with the pure system. Consequently with this, we obtained by means of the DFT calculations the electronic, optical and magnetic properties, like band gap and absorption coefficient of a ZnS system zincblende type including a dopant factor of 3.2% Ni, substitutional of Zn, adopting the experimental value for the cell parameter. In the theoretical calculation we obtained the optimized U value for Ni atoms by the inclusion of the Hubbard potential.

2. Experimental setup

Ni-doped ZnS nanoparticles were synthesized by wet bench method using zinc acetate ($Zn(CH_3COO)_2$), sodium sulphide (Na_2S), and the doping metal ion was obtained from nickel chloride ($NiCl_2$). The product was washed with ethanol and water, dried overnight at 60 °C, and stored in desiccators until subjected to further studies. The synthesis in this work was carried out without any capping reagent (chemical synthesis with capping agent that has a disadvantage like purity and yield), and with less sulphur concentration that conventional techniques. Zinc acetate, sodium sulphide and nickel chloride were procured and used for experiment without any further purification. Stock solutions of zinc acetate (0.1 M) and nickel chloride (0.01 M) were prepared previously and stored in airtight dark bottles that were used for synthesis. Sodium sulphide (0.01 M) solution was prepared freshly just before experiment, to avoid the loss of sulphide ion as hydrogen sulphide gas. During synthesis, 5 ml of zinc acetate solution was taken in a beaker and stirred for 10 min 3 ml of nickel chloride was added and continued stirring for 15 min for thorough mixing and distribution of ions. Sodium sulphide solution was added dropwise (0.2 ml per min) to the metal ion mixture with constant stirring. Sulphide ions forms seed crystals with excessive zinc ions and as reaction continues overnight. Before addition of sodium sulphide, mixture was transparent and in addition the reaction mixture turns milky white, finally grey precipitate is obtained. Precipitate was washed with water and alcohol to remove the organic and inorganic impurities. The pure Nano particles were dried at 600 C in an oven and stored in an airtight desiccator. The total yield of the reaction was 70%. Experimentally, the doping concentration of Ni was 3%. Further details can be found in [7]). The structural characterization and phase identification are carried out by: x-ray diffractometry (XRD), high resolution transmission electron microscopy (HR-TEM), and x-ray photoelectron spectroscopy (XPS) techniques. For XRD analysis, a Rigaku Miniflux II x-ray diffractometer with Cu-$K\alpha$ source was used (operating at 30 mA and 40 KV), the HR-TEM images were obtained using JOEL JEM 200 with high-resolution detectors (images recorded from 50 to 2 nm scale), and the XPS analysis was carried out using the Axis Ultra 165 instrument with Al-$K\alpha$ as the x-ray source with energy up to 1486 eV.

3. Theoretical methodology

The results were obtained within the Density Functional Theory (DFT) formalism, using the GGA approximation scheme for the exchange and correlation potential given by Perdew, Burke and Ernzerhof (PBE) [14] and the projector augmented wave (PAW), as implemented in the ABINIT package [15].It is well known that GGA method presents some limitations when applied to strongly correlated systems (like the 3d state from Zn, and 3d of Ni), and it is necessary to implement some method of correction of on-site Coulomb repulsion. Therefore, we employed the Hubbard effective U (U_{eff}). From the literature, it is known that for 3d Zn states the value of 8.0 eV is widely accepted in the ZnS system [16, 17], while for 3d-Ni states there is not an agreement about the correct value, so we performed an optimization study around different values between 0 and 8 eV for this potential. In both systems (pure and Ni-doped), the considered structure was a supercell that included 64 atoms (8 unit cells). For the Ni-doped ZnS system, we used the configuration shown in figure 1, where 31 Zn atoms, 32 S atoms and 1 Ni atom are represented which produced a doping concentration of 3.125%, consistent with experimental doping concentration. The used lattice parameter was experimentally obtained (5.364 Å, see section 4.1). All the calculations included spin polarization without spin orbit coupling [17].

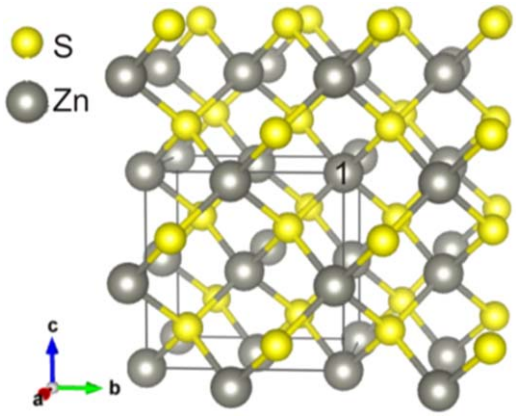

Figure 1. (a) The zinc-blende ZnS supercell ($2 \times 2 \times 2$) employed to define the model of pure ZnS and Ni-doped ZnS structure. The position of Zn substituted by Ni is denoted by 1. Continuous lines indicate the corresponding unit cell. (b) Band Structure of Ni:ZnS with 3% dopant, where the black lines refer to spin up, and red lines to spin up.

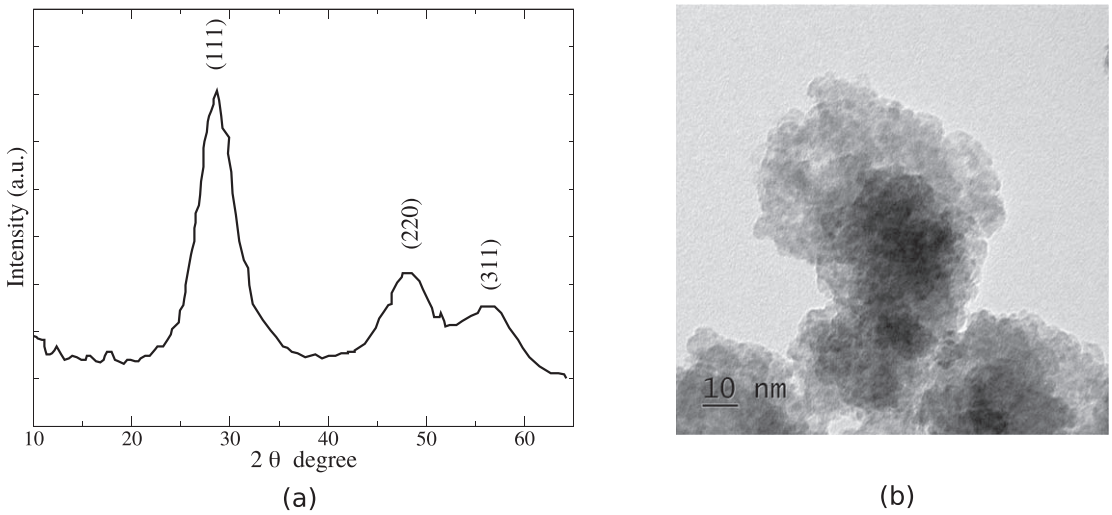

Figure 2. (a) XRD pattern of Ni-doped ZnS nanoparticles, the indicated diffraction peaks correspond to lattice planes and are in agreement with the PCPDF# chart of cubic ZnS. (b) Selected HR-TEM image of the synthesized Ni-doped ZnS nanoparticles.

4. Results and discussion

4.1. Morphological and structural characterization of Ni-doped ZnS nanoparticles

The crystallinity and crystal size of Ni-doped ZnS nanoparticles were determined on the basis of x-ray line broadening and calculated by Debye–Scherrer formula [18]. XRD pattern is shown in figure 2(a), the observed diffraction peaks correspond to (111), (220), (311) lattice planes, and are well matched with the standard of cubic ZnS (ICSD #60378). The estimated average size of the crystallites and lattice parameter (lattice spacing) indicate 8nm and 5.364 Å, respectively. HR-TEM analysis was carried out for Ni-doped ZnS nanoparticles by dispersing in methanol and spreading it on carbon coated copper grid. Nanoparticles were analyzed at various magnifications, and a selected image is shown in figure 2(b). As can be seen, the nanoparticles are irregular shape, because no capping agents were used during synthesis). An analysis of the particle size distribution determined an average diameter of 8 ± 1 nm, in total agreement with the observed by XRD. Nanoparticle with less than 100 nm is considered as quantum dot and the Bohr's radius is 2.5 nm.

4.2. Electronic characterization

The DFT plus the Hubbard U correction approach (DFT+U) depends crucially on the choice of the local Coulomb interaction parameters, that are often chosen empirically. Nevertheless, no consensus has been reached about the optimal parameter in Ni-doped ZnS system [19–21]. Thus, we develop a study to determine which is the best value to the U_{eff} term of Ni atoms, while for Zn atoms, we used the widely accepted value of

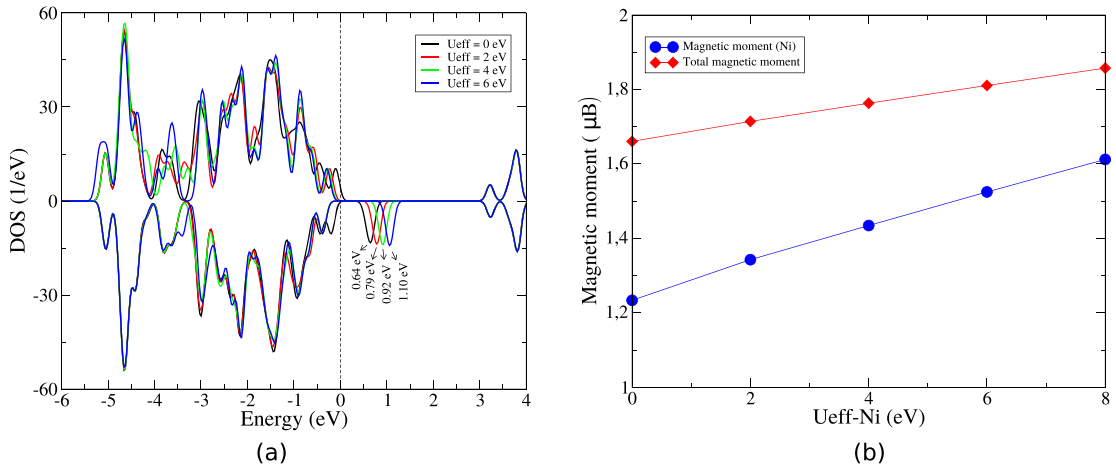

Figure 3. (a) Spin-resolved Total DOS of Ni:ZnS for different values of Ueff-Ni. (b) Magnetic moment of Ni (circle), and total magnetic moment (diamond) as a function of Ueff-Ni.

8 eV [18]. Figure 3(a) shows the spin-polarized density of states (DOS) for the Ni:ZnS system, calculated using different U_{eff} values on Ni 3d states. As seen in the DOS plots, the cation substitutional Ni-doping induces impurity bands in the band gap, which are strongly dependent on the U_{eff}-Ni used for the calculations. An increase of U_{eff}-Ni produces a greater splitting of the impurity band, represented on a shift of approximately 0.40 eV of the impurity band between U_{eff}-Ni from 0 to 6 eV.

Also, in figure 3(b) it is shown the magnetic moment dependence of Ni (blue line), and total magnetic moment per supercell (red line) as a function of U_{eff} value used for the U correction. In the formation of the total magnetic moment contribute mainly the Ni dopant and its nearest neighboring S atoms, which are ferromagnetically coupled to each other.

Since the effective potential U_{eff} is a semiempirical value, to determine its optimal value, it is necessary to compare the calculated values of some physical properties with their corresponding measured results. For this, the optical properties for different U_{eff}-Ni values were calculated, and compared with the corresponding experimental results. The experimental band gap reported was 3.85 eV, while the calculated value was 2.95 eV, therefore, in the calculation of optical properties, the correction was considered by the so called scisor operator of 0.90 eV. In order to obtain the optimal value U_{eff}-Ni, we compared the theoretical DOS with experimental results obtained by XPS on the energy region between −5 to 0 eV, energy range for which the d-Ni orbitals have the greatest contribution to the XPS spectrum. Thus, in figure 4(a) we presented the fitting of the total DOS for each U_{eff} value compared to the XPS obtained for the same energy range (the total DOS is the sum of the density of states spin up and spin down). It can be seen that the DOS curve of $U_{eff} = 4$ eV (green dotted line) is the nearest to experimental curve (black dotted line). Therefore, and for the rest of the calculations, we used the value of $U_{eff} = 4$ eV for Ni atoms on the Hubbard correction, and to equilibrate a structure to its lowest energy configuration, the atomic positions of the Ni, and their first and second neighbors, were allowed to relax until the residual forces on the atoms were less than 5×10^{-3} $Ha/Bohr$. Figure 4(b) is the XPS obtained for a wide energy range.

The band structure of Ni:ZnS with 3% dopant has been calculated and shown in figure 5, where the zero point (blue dashed line) denotes the Fermi level (E_F), so the negative and positive values indicate the valence band (VB) and conduction band (CB), respectively. The band gap reported was 2.95 eV. The Ni dopant have effects on band structure where the impurity level is above the E_F (0.87 eV).

To investigate the stability of doped ZnS, the defect formation energy (E_{Form}) was calculated according to the following expression [22–24]:

$$E_{Form} = E_{doped} - E_{pure} - \mu_{host} - \mu_X \quad (1)$$

where E_{doped} and E_{pure} are the total energy of the ZnS supercell with and without the Ni dopants, while μ_X and μ_{host} are respectively the chemical potentials of the substitutional atom Ni and of the substituted Zn host atom. The chemical potentials depend on the growth conditions and the source of atoms involved in the process (variations between S-rich and Zn-rich growth condition). Using the same method as [22, 23], we assume μ_{Zn} and μ_S in thermal equilibrium with ZnS ($E_{ZnS} = \mu_{Zn} + \mu_S$), and we also consider formation energy of ZnS itself (E_{Form} [ZnS] $= \mu_{ZnS} - \mu^0_{Zn} - \mu^0_S$). The chemical potential of the Ni dopant was calculated with respect to bulk-FCC structure. Thus, under Zn-rich condition ($\mu_{Zn} = \mu^0_{Zn}$),the formation energy for Ni-doped ZnS obtained was 3.951 eV, while under S-rich condition ($\mu_{Zn} = E_{Form}$ [ZnS] $+ \mu^0_{Zn}$), the corresponding formation energy

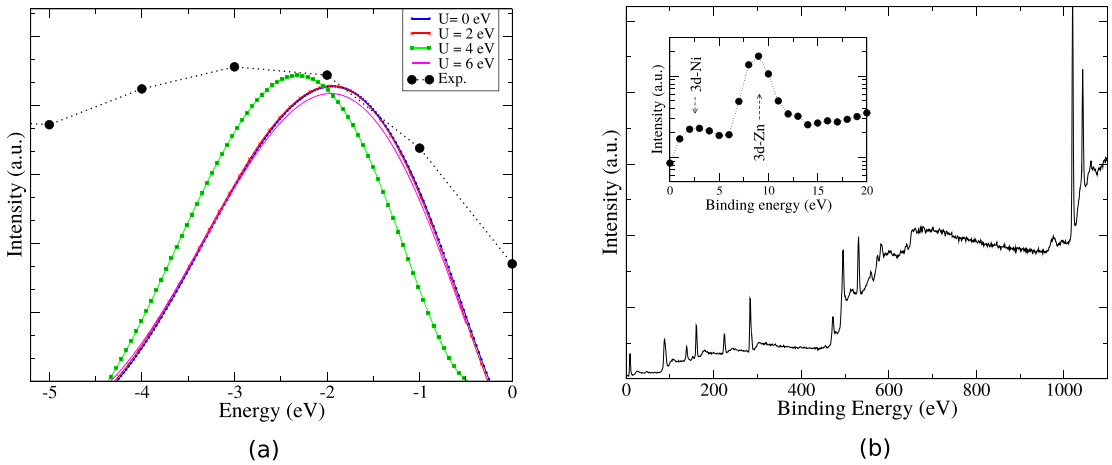

Figure 4. (a) Theoretical and experimental comparison between the total DOS and spectrum XPS for the energy between 0 eV and 5 eV. We display the fitting of the total DOS for each U value. (b) Wide survey spectrum of Ni:ZnS with XPS. The inset shows a zoom (in logarithmic scale) into the energies of interest for the estimation of the effective U.

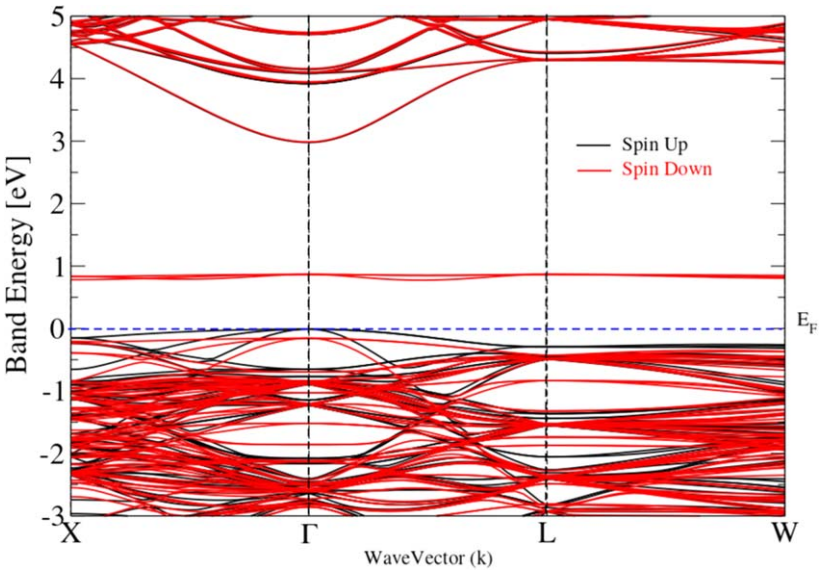

Figure 5. Band Structure of Ni:ZnS with 3% dopant, where the black lines refer to spin up, and red lines to spin up.

was −13.324 eV. The latter indicates that under S-rich growth condition (or Zn-poor condition), substitutional doping will occur easily in ZnS (or even form spontaneously), which is reasonable due to the presence of Zn vacancies in ZnS grown under these conditions.

Figure 6(a) shows the total DOS (TDOS) of pure and Ni-doped ZnS systems. In the case of the pure system, we performed the calculations using a supercell of dimensions equal to the one of to the doped system (64 atoms), and with the same lattice parameter (experimental data of the Ni:ZnS sample). This allows to distinguish between effects specific to doping, maintaining the same residual stress in the system. As can be seen, the presence of the Ni atom induces an impurity band above the Fermi level at 0.87 eV for spin down DOS. Since the presence of these states on the band gap region can be recombination centers or trapps, the probable transitions due to the presence of the doping atoms are also indicated in the figure, 0.87 eV, 2.31 eV, and 2.84 eV. In the inset of the figure 6(a), we presented the three main structures formed in the whole valence band region; a peak at −13.4 eV originating from the s-S orbitals, a sharp peak at −9.0 eV deriving from the d-Zn orbitals, and another broad structure from about −5.5 eV up to the Fermi energy, mainly due to the p-S orbitals, but containing also some contribution from p-Zn, s-Zn and d-Ni orbitals.

In order to identify the orbitals that contribute to the impurity band in the Ni-doped ZnS, we calculate the partial densities of states (pDOS) of Ni and their nearest neighbors. We showed this in figure 6(b), deploying the pDOS of Ni, S, and Zn atoms. While in the impurity band, the main intervening orbitals are d-Ni (figure 6(b)-

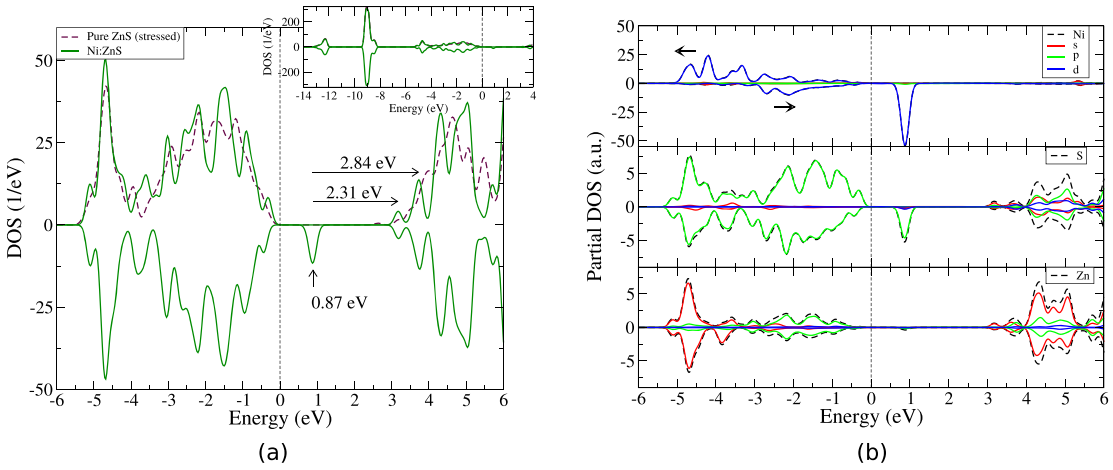

Figure 6. (a) Spin-resolved TDOS for pure ZnS compared with Ni-doped ZnS system. (b) Spin-resolved partial DOS of Ni (top), S atom (middle) , and Zn atom (bottom).

top) and p-S (figure 6(b)-middle), and the contribution of Zn states is negligible on the band gap zone, (figure 6(b)-bottom). Our results are in total agreement with experimental data presented by Saikia *et al* [25] who reported that Ni-doped ZnS have a high sp-d hybridization between orbitals sp form the valence band edge of ZnS and d orbitals from Ni^{2+} ions. Xiao *et al* [26] developed a DFT study and found that ZnS crystals have a weak ferromagnetic behavior, while from experimental results Saikia *et al* found that the presence of Ni^{2+} produces a ferromagnetic behavior at room temperature.

In figure 7, we displayed the spin density of the Ni:ZnS system. With the aim to analyze the effect of Ni atom in the charge density of its nearest neighbors, we calculated spin-polarization density difference (local magnetic moment) for six planes: L_3, L_2, L_1, L_0, L_{-1}, L_{-2} (see figure 7). The L_0 plane is localized across the Ni atom, L_1 and L_{-1} are planes between the atoms of S and Zn(Ni), L_2 and L_{-2} are planes containing the S atoms, and L_3 plane across to the Zn atoms. As seen in figure 7, the local magnetic moment is strongly localized in Ni-dopant atom (~80% of the total magnetic moment, see figure 3(b)), and this induces a polarization of its nearest neighbors. The L_1 and L_{-1} planes exhibit the spin distribution due to the hybridization between the Ni atom and its first neighbors (S atoms), while the L_2/L_{-2} and L_3 planes present the spin distribution induced in S and Zn atoms, respectively. The L'_0 and L'_{-1} planes in the (111) surface show that the spin distribution is mainly due to the hybridization between the Ni atom and the S atoms.

4.3. Optical properties

The optical properties were calculated using the energy values of 4 eV and 0.9 eV for the Hubbard correction and the scissor operator, respectively. Figure 8(a) shows the results of the imaginary part of the dielectric function (ε_2) as a function of energy before and after doping with Ni (to isolate the contribution of stress and doping defects). This allows us to distinguish between effects of the doping element and those that produce the defect the lattice structure. As shown in figure 8(a), the influence of Ni atom is mainly given at low energy regions ($E < 6$ eV). It can be seen that there are two main peaks in the imaginary part of the dielectric function in the Ni-doped ZnS system, the energies of peaks are 0.97 eV and 2.22 eV, respectively. According to the density of states shows in figure 6(a), the peak located at 0.97 eV is mainly caused by the transition between p-S orbital in the highest valence band and impurity band states (d-Ni and p-S states). The peak located at 2.22 eV is mainly derived from transition from impurity band states to conduction band. It can also be observed that the difference of the ε_2 between pure and doped ZnS lies mainly on the intensity and location of the peaks. Compared to the pure ZnS, in the Ni-doped ZnS system the increasing in the peaks intensity is attributed to the increasing of the local carriers concentration which increases the transition probability. From this dielectric function, by applying the Kramers and Kronig relationships, it was possible to determine the remaining optical properties, the absorption coefficient, the refractive index, and the extinction coefficient.

The refractive index of the pure and doped systems in the energy range of 0–20 eV are shown in figure 8(b). It can be seen that the peak value of the refractive index increases and the main peaks move to the high energy after doping. For the Ni:ZnS system, the low energy range (<7 eV) is characterized by large refractive index and the 8 eV–20 eV range is characterized by small refractive index.

In figure 9 are represented the absorption coefficient and the extinction coefficient calculated for pure and Ni-doped ZnS compared with experimental results. For the latter, the experimental values were normalized to their value at 200 nm. From figure 9(Left), at short wavelengths, the absorption coefficient for Ni:ZnS system

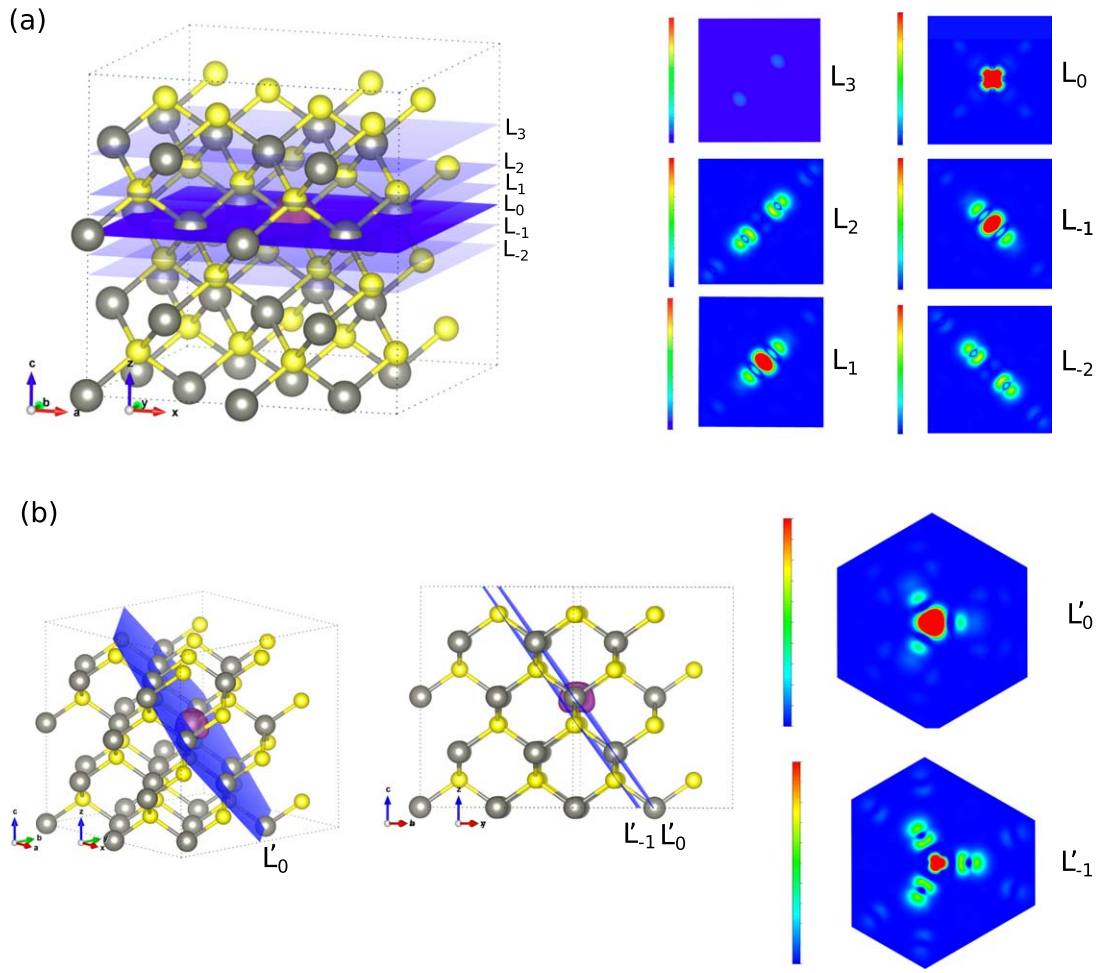

Figure 7. Spin density of the Ni:ZnS system (a) (001) surface and (b) (111) surface. (a) Spin-polarization density difference (local magnetic moment) for six planes: L_3, L_2, L_1, L_0, L_{-1}, L_{-2}. The L_0 plane is localized across the Ni atom, L_1 and L_{-1} are planes between the atoms of S and Zn(Ni), L_2 and L_{-2} are planes containing the S atoms, and L_3 plane across to the Zn atoms. (b) Spin-polarization density difference for two planes: L'_0 and L'_{-1}. L'_0 plane is localized across the Ni atom and show the spin density of Ni-Zn bonding; L'_{-1} plane containing the S atoms.

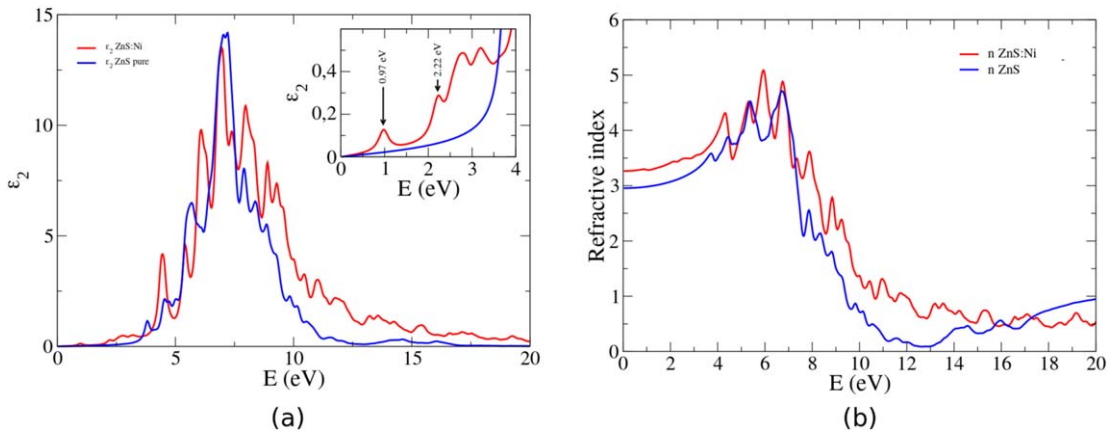

Figure 8. (a) Imaginary part of dielectric function for Ni:ZnS system between 0 and 20 eV. (Inset) Zoom between 0 and 4 eV to show the values of principal peaks. (b) Calculated refractive index for Ni:ZnS between 0 and 20 eV.

presents three marked regions of strong absorption between 6.2 eV(200 nm) and ~3.9 eV (320 nm), showing a splitting in absorption peak around 4.13 eV (300 nm), in good agreement with experimental results (we used the Tauc plot representation). Theoretically the dopant affect the absorption spectrum in the low and high energy range.

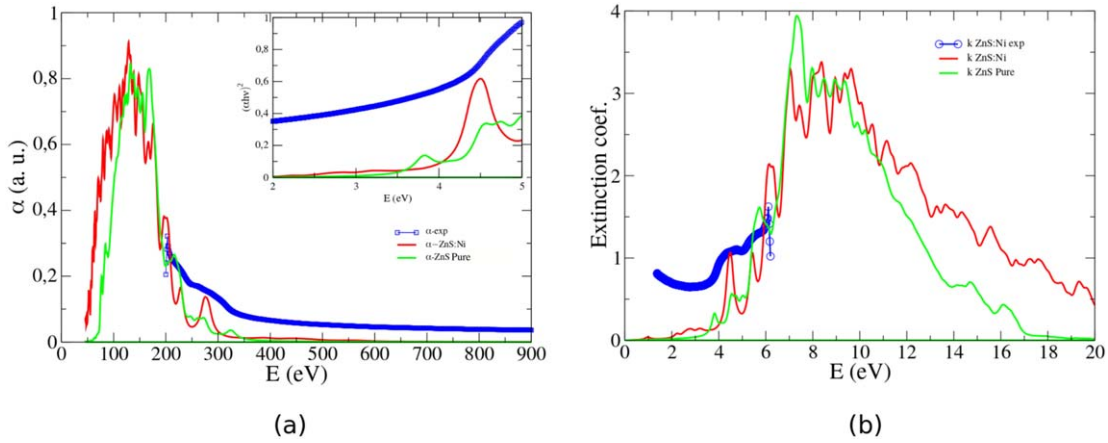

Figure 9. Experimental and theoretical (a) absorption coefficient inset(Tauc plot representation) and (b) extinction coefficient; stressed ZnS (red line) and Ni:ZnS (green line) systems.

On the other hand, form the experimental work we report photoluminescence measurements from optical excitation with 254 nm (4.88 eV), finding an emission at 430 nm (2.88 eV), which is typical in ZnS crystal. Furthermore, an emission at 412 nm (3.01 eV) that is associated with doping Ni, and at 453 nm (~2.74 eV), which is associated with recombination sites. In previous reported works, Saikia *et al* showed the absorption coefficient for different rates of Ni doped and found different peaks at 305 nm, 309 nm and 315 nm for 1%, 3% and 5% of dopant respectively, they found a red shifted with the increase of dopant concentration and said that this could be due to the strong sp-d interaction between ZnS Band electrons and d Ni orbitals.

5. Conclusion

We presented a theoretical and experimental study of the electronic and optical properties of the Zinc sulphide doped with nickel. Our results indicate that the presence of Ni atom make necessary the use of the Hubbard correction to include the effect of d states, for this, for the experimental and theoretical comparison, we show that the value of U that are close to experimental XPS is 4 eV. Besides, considering the dependence of the magnetic moment of the system shown on figure 3(inset), we consider that a U_{eff}-Ni close to 4.0 eV reproduces the magnetic moment of the atomic Ni in an accurate form. On the other hand, we obtain that Ni atoms contribute to a: (i) splitting of bands on the band gap energy region —orbitals 3d-Ni—, and, (ii) the change of the density of states to both up and down spin states in the valence band. The spin density of the Ni:ZnS system show that the local magnetic moment is strongly localized in Ni-dopant atom and this induces a polarization of its nearest neighbors. A comparison between dielectric function (ε_2) for system with and without dopant showed the influence of Ni atom is mainly given at low energy regions ($E < 6$ eV). In photoluminescence measurements from optical excitation with 4.88 eV (254 nm), we reported an emission at 2.88 eV (430 nm), which is typical in ZnS crystal. Furthermore, an emission at 3.01 eV (412 nm) that is associated with doping Ni, and at ~2.74 eV (453 nm), which is associated with recombination sites. These results show that inclusion of impurities of transition metals like Ni at low concentrations (less than 3%), causes significant changes on electric, optical and magnetic properties of host material (ZnS), and induce the apparition of trap levels on the gap regions. These make the material have adquire ferromagnetic behaviors, important to tune magnetic, electrical and optical properties of laser, optical, photoluminescent or spintronic devices. Our results show that the formation energy in Ni-doped ZnS system is largely dependent on the growth conditions.

Acknowledgments

The authors acknowledge financial support from the Consejo Nacional de Investigaciones Científicas y Técnicas (CONICET) and the Universidad Nacional de Entre Ríos (UNER).

ORCID iDs

S Rodríguez https://orcid.org/0000-0002-4110-4469

References

[1] Kumar S *et al* 2013 Room temperature ferromagnetism in Ni doped ZnS nanoparticles *J. Alloys Compd.* **554** 357–62
[2] Reddy D A, Murali G, Vijayalakshmi R P and Reddy B K 2011 Room-temperature ferromagnetism in EDTA capped Cr-doped ZnS nanoparticles *Applied Physics A: Materials Science and Processing* **105** 119–24
[3] Ma X, Song J and Yu Z 2011 The light emission properties of ZnS:Mn nanoparticles *Thin Solid Films* **519** 5043–5
[4] Lun Y, Lin Y, Meng Y and Wang Y 2014 CdS quantum dots sensitized ZnO spheres via ZnS overlayer to improve efficiency for quantum dots sensitized solar cells *Ceram. Int.* **40** 8157–63
[5] Maji S K, Dutta A K, Srivastava D N, Paul P, Mondal A and Adhikary B 2011 Effective photocatalytic degradation of organic pollutant by ZnS nanocrystals synthesized via thermal decomposition of single-source precursor *Polyhedron* **30** 2493–8
[6] Ummartyotin S and Infahsaeng Y 2016 A comprehensive review on ZnS_ From synthesis to an approach on solar cell *Renew. Sustain. Energy Rev.* **55** 17–24
[7] Vadiraj K T and Belagali S L 2016 Synthesis and optical characterization of nickel doped zinc sulphide without capping agent *J. Mater. Sci., Mater. Electron.* **27** 2885–9
[8] Yin Z H, Zhang J M and Xu K W 2016 Structural, electronic and magnetic properties of transition metal atom-doped ZnS dilute magnetic semiconductors: a first-principles study *Mater. Chem. Phys.* **183** 201–9
[9] Soni H, Chawda M and Bodas D 2009 Electrical and optical characteristics of Ni doped ZnS clusters *Mater. Lett.* **63** 767–9
[10] Bera K, Saha S and Chandra Jana P 2018 Investigation of structural and electrical properties of ZnS and Mn doped ZnS nanoparticle *Materials Today: Proceedings* **5** 6321–8
[11] Matxain J M, Fowler J and Ugalde J 2000 Small clusters of II–VI materials:ZniSi *Phys. Rev.* A **61** 053201
[12] Chen H, Shi D, Qi J and Wang B 2011 First-principles study on the magnetic properties of transition-metal atoms doped (ZnS)12 cluster *J. Magn. Magn. Mater.* **323** 781–8
[13] Fang X, Zhai T, Gautam U K, Li L, Wu L, Bando Y and Golberg D 2011 ZnS nanostructures: from synthesis to applications *Prog. Mater Sci.* **56** 175–287
[14] Perdew J P, Burke K and Ernzerhof M 1996 Generalized gradient approximation made simple *Phys. Rev. Lett.* **77** 3865–8
[15] Gonze X *et al* 2009 ABINIT: First-principles approach to material and nanosystem properties *Comput. Phys. Commun.* **180** 2582–615
[16] Karazhanov S, Ravindran P, Grossner U, Kjekhus A and Svensson B G 2006 Electronic structure and band parameters for Zn X (X = O, S, Se, Te) *J. Cryst. Growth* **287** 1–6 Electronic structure and band parameters for Zn X (X=O, S, Se, Te)
[17] Karazhanov S, Ravindran P, Kjekhus A, Fjellvag H H and Svensson B G 2007 Electronic structure and optical properties of Zn: a density functional study *Phys. Rev. B* **75** 1–14
[18] Karazhanov Z, Ravindran P, Kjekshus A, Fjellvag H, Grossner U and Svensson B 2009 Coulomb correlation effects in zinc monochalcogenides *J. Appl. Phys.* **100** 043709
[19] Xie H Q, Tang L J, Tang J L and Peng P 2015 Magnetic properties of NI-doped ZnS: first-principles study *J. Magn. Magn. Mater.* **377** 239–42
[20] Akhtar M S, Malik M A, Riaz S and Naseem S 2015 Room temperature ferromagnetism and half metallicity in nickel doped ZnS: experimental and DFT studies *Mater. Chem. Phys.* **160** 440–6
[21] Aras M and Kilic C 2014 Combined hybrid functional and DFT+U calculations for metal chalcogenides *J. Chem. Phys.* **141** 044106
[22] Lu S, Li C, Zhao Y F, Gong Y Y, Niu L Y and Liu X J 2016 Tunable redox potential of nonmetal doped monolayer MoS_2 : first principle calculations *Appl. Surf. Sci.* **384** 360–7
[23] Dolui K, Rungger I, Das Pemmaraju C and Sanvito S 2013 Possible doping strategies for MoS_2 monolayers: An *ab initio* study *Phys. Rev.* B **88** 075420
[24] Zandalazini C and Albanesi E A 2019 *Ab initio* study on the role of the crystalline symmetry in the stabilization of the magnetic order in Al-doped SnS *J. Magn. Magn. Mater.* **484** 146–53
[25] Saikia D and Borah J 2017 Investigations of doping induced structural, optical and magnetic properties of Ni doped ZnS diluted magnetic semiconductors *Journal of Materials Science Materials in Electronics* **28** 1–10
[26] Xiao W, Wang L, Rong Q, Xiao G and Meng B 2014 Magnetism in undoped ZnS studied from density functional theory *J. Appl. Phys.* **115** 1–10